의학박사 학위논문

Changes in Osteoblast Differentiation and Gene Expression Profile of Mouse Bone during Mechanical Unloading

기계적 무부하가 쥐 조골세포 분화 및 유전자 발현 양상에 미치는 변화

2021 년 2 월

서울대학교 대학원

의학과 중개의학 분자유전체학 전공

홍 아 람

Changes in Osteoblast Differentiation and Gene Expression Profile of Mouse Bone during Mechanical Unloading

지도 교수 김 상 완

이 논문을 의학박사 학위논문으로 제출함
2020 년 10 월

서울대학교 대학원
의학과 중개의학 분자유전체학 전공
홍 아 람

홍아람의 의학박사 학위논문을 인준함
2021 년 1 월

위 원 장 신 찬 수 (인)

부위원장 김 상 완 (인)

위 원 이 재 협 (인)

위 원 최 무 림 (인)

위 원 백 기 현 (인)

Abstract

Changes in Osteoblast Differentiation and Gene Expression Profile of Mouse Bone during Mechanical Unloading

A Ram Hong

Translational Medicine, Molecular Genomic Medicine

School of Medicine

The Graduate School

Seoul National University

Background and purpose: Mechanical unloading induces reductions in bone and muscle mass, however, its cellular and molecular mechanisms have not been fully elucidated. Therefore, to better understand the effect of unloading on bone loss, we examined the conversion of active mature osteoblasts to bone lining cells (BLCs) via a lineage tracing study. In addition, we investigated RNA seq-based transcriptome profiling to capture genetic changes associated with mechanical unloading.

Methods: *Dmp1*-CreERt2 mice were crossed with Rosa26R mice to render targeted mature osteoblasts and BLCs. *Dmp1*-CreERt2(+):Rosa26R transgenic mice were injected with 1 mg of 4-hydroxy-tamoxifen (4-OHTam) three times a week from postnatal week 7. We developed a unilateral hindlimb unloading model. Briefly, the animals underwent a combination of botulinum toxin injection (2U/100 g) with left hindlimb tenotomy from postnatal week 8 to 10. The animals were euthanized at postnatal weeks 8, 9, 10, and 12 (i.e., 2 days, 1 week, 2 weeks, and 4 weeks after last 4-OHTam administration, n=4–6 in each group). The number and thickness of X-gal

(+) cells on the periosteal surface of both femoral bones were quantified at each time point. Further to this, we performed RNA-seq on pairs of femurs at each time point for wild-type (C57BL/6) mice euthanized at postnatal weeks 8, 10, and 12 using the same experimental protocol (n=3 per group at postnatal weeks 8 and 12; n=2 per group at postnatal week 9).

Results: Unilateral hindlimb unloading induced a significant reduction in femoral bone mass from 1 to 4 weeks following unloading. At 2 weeks after unloading (postnatal week 10), a significant decrease in the number of X-gal (+) cells and a subtle change in the thickness of those cells were observed in the left hindlimbs compared to the right hindlimbs (non-unloaded controls). At 4 weeks after unloading (postnatal week 12), the decrease in the thickness of X-gal (+) cells was accelerated in the left hindlimbs, while the number of X-gal (+) cells was comparable between both hindlimbs. RNA-seq analysis revealed downregulation of 315 genes in the unloaded hindlimbs at 2 and 4 weeks after mechanical unloading. Gene set analysis and protein-protein interaction network analysis identified potential interactions among differentially expressed genes related to glucose metabolism and calcium signaling. Of these, nine genes (i.e., *Xirp2*, *AMPD1*, *NEXN*, *Ppp1r3c*, *Mettl11b*, *Tceal7*, *CYP2E1*, *Bche*, and *Gadl1*) were upregulated during osteoblastogenic, myogenic, and osteocytic differentiation by quantitative real-time polymerase chain reaction *in vitro*.

Conclusion: The present study demonstrates that mechanical unloading can accelerate the conversion of active mature osteoblasts to BLCs in the early phases of bone loss *in vivo*. In addition, some of the genes related to this process may have a pleiotropic action on both bone and muscle, which may be useful to identify drug targets with dual effects for osteoporosis and sarcopenia.

Keywords: Mechanical unloading, bone lining cell, gene expression profiling, transcriptome

Student number: 2014-30933

Some data from this paper were published in Endocrinol Metab (Seoul) 2020;35:456-469.

CONTENTS

LIST OF TABLES

LIST OF FIGURES

Introduction

The skeleton allows land-dwelling vertebrates to engage in physical activities such as movement. During exercise or physical activity, mechanical forces are applied to the bones by gravity and contraction of skeletal muscles [1-3]. In particular, because skeletal muscles are tightly attached to the bones, loss of muscle mass or strength reduces the mechanical force on the bone, consequently contributing to bone loss [4,5]. In human studies, large changes in serum bone turnover markers and the loss of cancellous and cortical bones were evident as a result of mechanical unloading to occur during prolonged rest or long space flight [6,7]; Studies in rodents have shown that bone formation and muscle mass decreased after tail suspension, while bone resorption increased [8-10]. A representative clinical example of bone mass reduction caused by mechanical unloading is disuse osteoporosis observed in patients with disabilities after stroke, and spinal cord or brain injury. Physiological aging, as well as pathological conditions, is associated with decreased muscle mass and strength [11,12] and consequently decreased bone mass [13,14]. However, the cellular mechanisms underlying the reduction in bone mass caused by mechanical unloading have not been fully revealed.

Bone lining cells (BLCs) are inactive osteoblasts that line the surface of bone and can be mobilized to form bone as sources of active osteoblasts. BLCs can be reactivated by bone-forming agents. Previously, we have shown that intermittent parathyroid hormone (PTH) or sclerostin antibody treatment can convert quiescent BLCs into active osteoblasts. Our osteoblast lineage tracing studies have shown that intermittent exposure to PTH treatment can also delay the conversion of mature osteoblasts into BLCs [15-17]. Mechanical loading can also activate BLCs.

Mechanical loading experiments in rats have shown that the surface area of lining cells decreases after a single mechanical loading session [18]. Therefore, we can propose the idea that mechanical unloading also affects BLCs. However, there is no direct data on this possibility.

Bone-muscle interactions involve complex molecular and biochemical cross-talk, as both bone and muscle are endocrine organs, rather than merely mechanical connections [19-21]. In addition, both osteoblasts and muscle cells differentiate from common progenitor cells (i.e., mesenchymal stem cells), and the occurrence of osteoporosis and sarcopenia increases with age. Thus, identification of pleiotropic genes that affect both bone and muscle mass may elicit potential therapeutic targets for the management of these diseases [22,23].

In the present study, we used an osteoblast lineage tracing study to investigate the conversion of active mature osteoblasts into BLCs in response to unloading of bone. Furthermore, we examined RNA-sequencing (RNA-seq)-based transcriptome profiling to provide a comprehensive database of genes implicated with mechanical unloading.

Methods

Development of hindlimb unloading protocol

Since the establishment of bone loss by mechanical unloading is the first step of this study, we tried to develop an effective unloading protocol by repeated experiments. Initially, full grown 12-week-old wild-type (C57BL/6) mice were used for analysis. Among several methods that can lead to unloading in animals (e.g., tail suspension, botulinum toxin injection, cast immobilization, or tenotomy), we chose botulinum toxin injection because of the convenience of the method.

According to previous studies, we injected a 50 μL of botulinum toxin (2 U/100 g) or equal dose of saline into both hindlimbs of mice (n=10–12 per group). Since no significant decrease in bone mass was observed at 1 week after unloading, Achilles tenonomy was added to induce apparent bone loss. Then, serial measurements of total body weight and bone mineral density (BMD) of mice were performed at 1-week intervals using dual-energy X-ray absorptiometry (DXA) *in vivo*. We performed second injection of botulinum toxin because we did not observe significant bone loss within 3 weeks after unloading.

At 6 weeks after unloading, total body weight was significantly reduced in unloaded mice through repeated experiments (both P<0.001; Figure 1A and B). However, total body BMD decreased only in the second experiment (P=0.052 in the first experiment and P<0.001 in the second experiment; Figure 1C and D) *in vivo*. Therefore, we measured right femoral BMD *ex vivo*, and then observed significant bone loss at 6 weeks after unloading in both experiments (P=0.004 and P<0.001, respectively; Figure 1E and F).

Figure 1. Developing an effective mechanical unloading protocol: changes in body weight and bone mineral density

Changes in body weight (g) from baseline to 6 weeks after unloading at both hindlimbs in the (A) first experiment and (B) second experiment. Changes in total body bone mineral density (BMD; g/cm^2) in the (C) first and (D) second experiment *in vivo*. Changes in right femoral BMD in the (E) first and (F) second experiment *ex vivo*. Data are expressed as mean±standard error (n=10–12 per group at each experiment). [a]P<0.05.

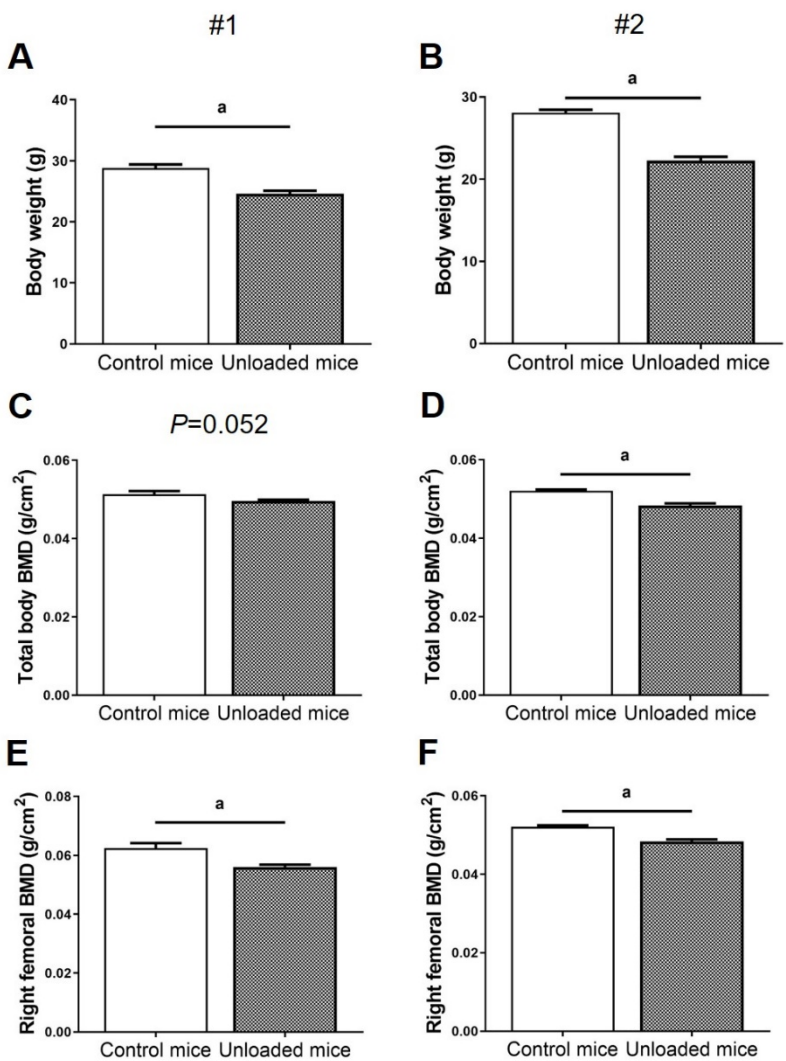

We measured serum levels of sclerostin and c-telopeptide of type 1 collagen (CTX) to assess changes in bone turnover status. The levels of serum bone turnover markers did not differ between unloaded and control mice through repeated experiments (Figure 2).

Figure 2. Developing an effective mechanical unloading protocol: changes in serum levels of bone turnover markers

Changes in serum levels of sclerostin in the (A) first experiment and (B) second experiment, and those of c-telopeptide of type 1 collagen (CTX) in the (C) first and (D) second experiment. Data are expressed as mean±standard error (n=10–12 per group at each experiment). [a]P<0.05.

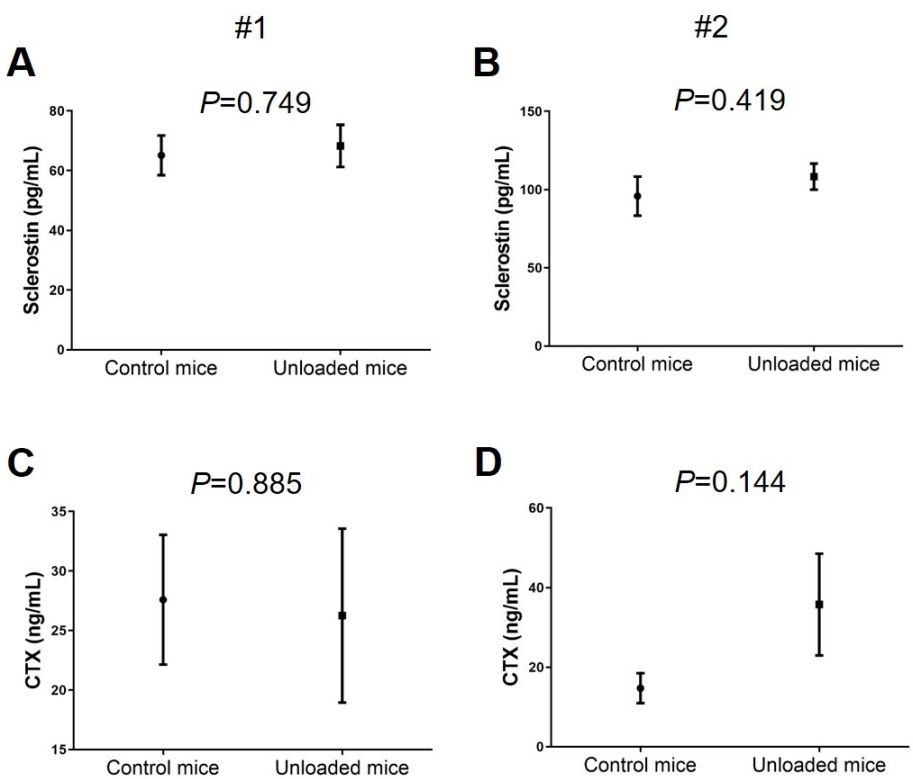

Mice

Postnatal 8, 9, 10, and 12-week-old wild-type (C57BL/6) mice were used for evaluating unloading-induced bone loss (*n*=8–10 per group), *SOST* mRNA expression of the femur (*n*=5 per group), and serum levels of bone turnover markers (*n*=15 per group). The mean body weight of mice euthanized at 8, 9, 10, and 12 weeks were 24.0 kg, 23.8 kg, 23.7 kg, and 27.1 kg, respectively.

We used a temporally-controlled transgene expression system to trace cells of the osteoblast lineage, called a lineage-tracing study [17]. In this system, when *Dmp1*-cyclic recombinase (Cre)ERt2 mice are crossed with Rosa26R mice, using a universally expressed promoter, Cre-mediated recombination induces *Escherichia coli* β-galactosidase expression [24]. Four to six postnatal weeks 8, 9, 10, and 12-week-old male and female mice were used for the lineage tracing study at each time.

We used postnatal weeks 8, 10, and 12-week-old wild-type (C57BL/6) mice to evaluate changes in mRNA expression in response to unloading under the same experimental protocol. Three male mice were used at each time point.

Survival rate was 100% in wild-type (C57BL/6) mice and 80% in *Dmp1*-CreERt2:Rosa26R mice.

There studies were approved by the Institutional Animal Care and Use Committee of Seoul National University (No. SNU-160513-3).

Tamoxifen administration

In *Dmp1*-CreERt2:Rosa26R mice, Cre-mediated recombination was induced by 4-hydroxy-tamoxifen (4-OHTam, Takeda, Japan) administration. A 2.5 mg of the 4-OHTam was dissolved in 100 μL of dimethylformamide (Thermo Fisher

Scientific, USA). Then this stock solution was diluted to 2.5 mg/mL of corn oil (Sigma-Aldrich, USA). Intraperitoneal injections with 1 mg of 4-OHTam were conducted in the *Dmp1*-CreERt2:Rosa26R mice three times a week initiating from postnatal week 7.

Experimental design of the study

Based on the results from previous attempts, in the current study, mechanical unloading was conducted on the left hindlimb by botulinum toxin injection in combination with Achilles tenotomy. In details, at postnatal weeks 8 and 10 of the mice, a 50 μL of botulinum toxin (2 U/100 g) was injected to the triceps surae, quadriceps, and calf muscles of the left hindlimb. The right hindlimb was injected by the same dose of normal saline and served as a non-unloaded control. At postnatal week 9, Achilles tenotomy was conducted on the left hindlimb (Figure 3).

We used 8-week-old mice at baseline for lineage-tracing of active mature osteoblasts on the periosteal surface. The animals were euthanized at postnatal weeks 8, 9, 10, and 12 (i.e., 2 days, 1, 2, and 4 weeks, respectively, after the last 4-OHTam administration in *Dmp1*-CreERt2:Rosa26R mice). Mice euthanized at postnatal week 8 (before unloading) served as controls for longitudinal analyses. RNA-seq-based transcriptome profiling used the same experimental protocol as a lineage-tracing study except that wild-type (C57BL/6) mice were used.

Figure 3. Experimental protocol of the study

Hindlimb unloading was achieved by botulinum toxin in combination with Achilles tenotomy in the left hindlimb. The right hindlimb served as the control. For a lineage

tracing study, *Dmp1*-CreERt2:Rosa26R mice were injected with 1 mg of 4-hydroxy-tamoxifen (4-OHTam) three times a week starting from postnatal week 7. Animals were euthanized at postnatal weeks 8, 9, 10, and 12 (i.e., 2 days, 1 week, 2 weeks, and 4 weeks after the last 4-OHTam injection) to capture the fate of active mature osteoblasts *in vivo*. For RNA-seq-based transcriptome profiling, wild-type (C57BL/6) mice were used under the same experimental protocol. Adapted from Hong et al. Endocrinol Metab (Seoul) 2020;35:456-469 [25].

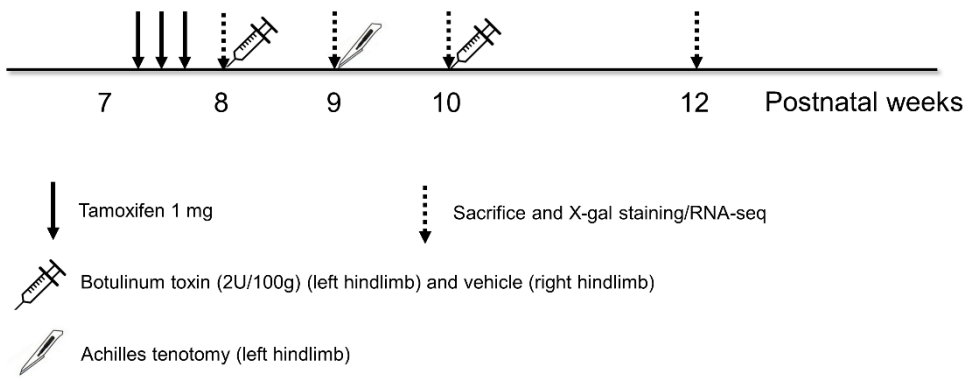

In vivo measurement of bone mass

At weeks 8, 9, 10, and 12 before euthanasia, the whole body and hindlimb BMD (g/cm^2) as well as bone mineral content (BMC; g) were measured *in vivo* by DXA using a PIXImus (GE Lunar, Madison, WI, USA). Mice were anesthetized using a 3:1 mixture of Zoletil (Virbac Laboratories, France) and Rompun (Bayer, Germany), then placed prone on the platform of a PIXImus scanner for BMD and BMC measurements. Eight to 10 mice were analyzed for each group at postnatal 8, 9, 10, and 12 weeks.

Ex vivo measurement of bone microarchitecture

After euthanasia, whole tibiae were harvested from the mice and fixed in formaldehyde solution for 48 hours. They were placed in 70% ethanol, then stored at 4°C until analysis. The proximal tibia of each mouse was scanned by high-resolution micro-computed tomography (μCT; SkyScan 1173, Bruker microCT) at 90 kV and 88 μA with an isotropic voxel size of 7.1 μm using a 1.0 mm aluminum filter. For the analysis of metaphyseal tibia, a 1.5-mm section which was started 500 μm below the growth plate was analyzed. Then, scanned images were reconstructed with NRecon v.1.6 software (Bruker microCT) by adjusting for beam hardening and ring artifacts. Data were analyzed using a CT analyzer. For trabecular bone regions of proximal tibiae, bone volume/total volume (BV/TV), trabecular number (Tb.N), trabecular thickness (Tb.Th), and trabecular separation (Tb.Sp) were measured. Eight to 10 mice were analyzed for each group at postnatal 8, 9, 10, and 12 weeks.

RNA extraction and quantitative real-time polymerase chain reaction for *SOST mRNA* expression of the femur

We evaluated the level of mRNA expression for *SOST* in the femur in response to mechanical unloading. Total RNA was extracted from femoral diphyseal bones of C57BL/6 mice at postnatal weeks 8, 9, 10, and 12 (n=5 per group). After isolation from the femur using TRIzol reagent (Invitrogen), total RNA was subsequently reverse transcribed with the Reverse Transcription System kit (Promega, USA). cDNA was amplified (Applied Biosystems, UK) with TaqMan (Applied Biosystems) or SYBR Green polymerase chain reaction (PCR) technology. A mouse-specific primer of *SOST* was used for the analysis. By quantitative real-

time PCR (qRT-PCR), we compared the relative *SOST* mRNA expression levels normalized to β-actin between unloaded and control femurs using a LightCycler 96 system (Roche Diagnostics, Manheim, Germany). Relative gene expression levels were calculated using the $2^{(-\Delta\Delta CT)}$ method.

Detection of serum levels of bone turnover markers

Before mice were euthanized, blood was collected by cardiac puncture. Aliquots of serum samples were stored at −80°C until analysis. We measured serum levels of N-terminal propeptide of type I procollagen (P1NP) as an index of bone formation, by enzyme-linked immunosorbent assay (ELISA) using P1NP ELISA kit (Mouse/Rat P1NP; Immunodiagnostics Systems, UK). Serum levels of sclerostin and CTX were measured as indices of bone resorption. Serum levels of sclerostin were measured using ELISA kits (Quantikine ELISA Mouse/Rat SOST; R&D Systems, USA) and those of CTX were measured using Ratlaps™ EIA kit (Immunodiagnostic Systems, UK). All measurements were performed according to the manufacturer's protocol. Fifteen mice were analyzed for each group at postnatal weeks 8, 9, 10, and 12 weeks.

5-bromo-4-chloro-3-indolyl-β-d-galactopyranoside staining, histological analysis, and quantification of labeled cell measurement

5-bromo-4-chloro-3-indolyl-β-d-galactopyranoside (X-gal) staining for activating β-galactosidase was performed to achieve lineage-tracing and quantification of X-gal (+) cells [15,16,26]. In details, both femurs were dissected from each mouse and soft tissues were removed before preparation. Each sample

was rinsed twice by phosphate-buffered saline (PBS) and fixed in 10% formalin at 4°C for 30 minutes. This was further washed three times with PBS and stained overnight at 37.8°C in X-gal solution which contains 1 mg/mL of X-gal (Takeda), 2 mM $MgCl_2$, 0.02% nonidet P-40, 0.01% sodium deoxycholate, 5 mM potassium ferrocyanide, and 5 mM potassium ferricyanide. Samples were decalcified with buffered ethylenediaminetetraacetic acid for 2 weeks, then embedded and processed for paraffin sections. Sections were counterstained with eosin. The X-gal (+) cells in the microscopic field of view from eight to 16 were counted from four to six comparable sections at ×400 magnification. Periosteal X-gal (+) cells in each femur were analyzed using a Leica Application Suite camera (DM 2500, Leica Microsystems, USA) and associated software (LAS v.3.8). Four to six mice were used for each group at postnatal weeks 8, 9, 10, and 12 weeks.

Statistical analysis of the lineage tracing study

All numerical data are expressed as mean±standard error. The Student *t* test was used to compare the effects of mechanical unloading between or within groups. Statistical analyses were performed using SPSS for Windows version 21 (IBM Corp., USA). We considered a $P<0.05$ statistically significant.

mRNA library preparation and sequencing

Transcriptome profiling used total RNA extracted from femoral diphyseal bones of C57BL/6 mice at postnatal weeks 8, 10, and 12 ($n=3$ per group). Immediately after sacrifice, the femur was dissected and adherent tissues were removed. After removing the proximal and distal epiphyses, the bone marrow was

flushed out using 1 mL of RNAlater solution (Ambion, USA). Using a tissue homogenizer, RNA was extracted from the femur homogenized in 1 mL of TRIzol reagent (Invitrogen, USA). Then, RNA was extracted from the homogenate and evaluated for purity and quantity using a spectrophotometer (Nanodrop 8000, Thermo Fisher Scientific). Total RNA quality was evaluated with a Bioanalyzer (Model 2100, Agilent Technologies, USA). Sufficient quality for sequencing library preparation indicates a RNA integrity number of 7 or higher.

The libraries were prepared for 100-bp paired-end sequencing using a TruSeq RNA Library Preparation kit (Illumina, USA). Using oligo (dT) magnetic beads, mRNA was purified and fragmented from 2 μg of total RNA. Then, the fragmented mRNAs were synthesized as single-stranded cDNAs via random hexamer priming, and subjected to a template for second-strand synthesis for preparation of double-stranded cDNA. The cDNA libraries were amplified using PCR after sequential end repair, A-tailing, and adapter ligation. Library quality was assessed with the BioAnalyzer 2100 and quantification was evaluated using the KAPA library quantification kit (Kapa Biosystems, USA). Paired-end sequencing (2×100 bp) was conducted on a HiSeq2500 instrument (Illumina) following cluster amplification of denatured templates.

Raw read processing

Using Trimmomatic, raw FASTQ files were trimmed with the following parameters: -threads 1 ILLUMINACLIP, LEADING:3 TRAILING:3 SLIDINGWINDOW:4:15 MINLEN:36 [27]. Then, these trimmed reads were aligned to the University of California at Santa Cruz *Mus musculus* mm10 reference

genome using STAR [28]. FeatureCounts was used to count the reads after alignment [29]. The count estimates were normalized with upper-quartile normalization.

Selection of differentially expressed genes

Initially, three pairs were sequenced for mice euthanized at postnatal weeks 8, 10, and 12 for transcriptome profiling analysis. However, principal component analysis (PCA) of the femur gene expression profile revealed a significant outlier in unloaded limbs at postnatal week 10 (Figure 4). Hence, we removed one mouse in week 10 in the analysis. Consequently, we used three mice at postnatal weeks 8 and 12, and two mice at postnatal week 10 for differentially expressed gene (DEG) analysis.

Figure 4. Principal component analysis for RNA sequencing data

Among unloaded limbs, one from 10-week-mice showed a poor quality for transcriptome analysis. Therefore, after excluding one mouse from postnatal week 10, DEG analysis was conducted in three mice at postnatal weeks 8 and 12 and two mice at postnatal week 10. By courtesy of Kwangsoo Kim. Modified from Hong et al. Endocrinol Metab (Seoul) 2020;35:456-469 [25].

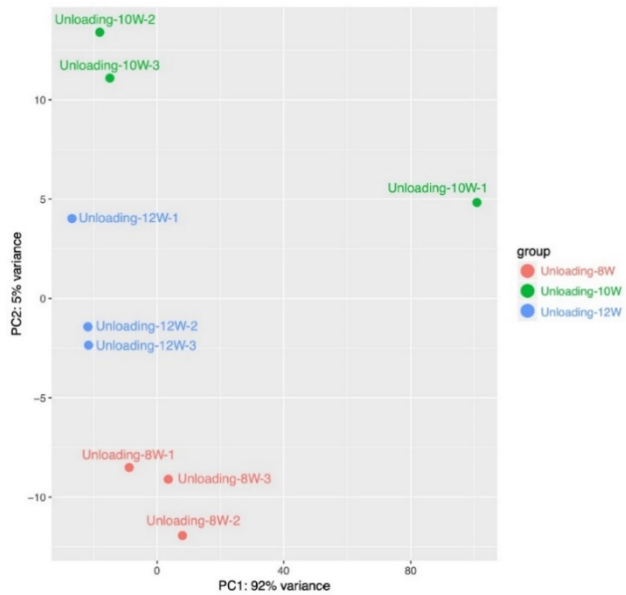

Paired RNA-seq data were obtained from the unloaded and control limb of each mouse. Log_2 fold changes (log_2FC [=log_2(unloaded hindlimb expression+1)/(control hindlimb expression+1)]) were calculated for all genes in each mouse. DEG analysis was conducted using eight log_2FC values derived from each gene. The log_2FC of each gene of mouse i in week j was referred to as $LFC_{i,j}$.

Due to the different number of mice, genes with $min_{i\in\{1,2\}}(|LFC_{i,10}|)>1.5$ and genes with $min_{i\in\{1,2,3\}}(|LFC_{i,12}|)>1.2$ and $average_{i\in\{1,2,3\}}(|LFC_{i,12}|)>1.5$ were determined as DEGs for postnatal weeks 10 and 12, respectively. In the DEG lists for postnatal weeks 10 and 12, DEGs at postnatal week 8 identified using the same criteria as week 12 were removed, since they have not been affected by mechanical unloading. Because week 10 included two mice and the other weeks were independent, we determined DEGs using the FC values without other statistical selection methods (e.g., the paired-*t* test or DESeq).

For all experimental datasets, genes whose read coverage was below 5 were excluded from the DEG analysis. To compute fold change, a pseudo-count of 1.0

was added to the expression values.

Gene set analysis and protein-protein interaction network analysis

Using Database for Annotation, Visualization and Integrated Discovery (DAVID), the DEGs were subjected to gene set enrichment analyses of gene ontology (GO) and Kegg pathways [30]. Using the Benjamini-Hochberg adjusted *P* value (q<0.05) of the Fisher exact test, significantly enriched gene sets were identified.

To further understand the biological relevance of DEGs, protein-protein interaction (PPI) network analyses of DEGs were performed based on the STRING database with Cytoscape (Ver3.7.2) STRING app (Confidence cutoff=0.4) and removed nodes with zero edge for downstream analysis [31]. We discovered meaningful subnetworks with EAGLE algorithm provided by Cytoscape ClusterViz app (CliqueSize Threshold=3 and ComplexSize Threshold=2) [32]. For subnetwork with highest modularity, we expanded network by adding 1 neighbor of each gene with Cytoscape CluePedia app [33]. Network expansion was performed based on the STRING DB edge link file from CluePedia, and 16 active interaction sources (Activation, Binding, Catalysis, Expression, Inhibition, Posttranslational modification, Co-expression, Combine, Fusion, Text-mining, Database, Experimental, Co-occurrence, Neighborhood) were used to select genes, without considering interaction scores. Gene set analysis was performed with Cytoscape ClueGO app and GO terms/Pathway results were filtered by following threshold: Benjamini-adjusted *P* value <0.05, 3 min Genes, and 4% Genes [34].

qRT-PCR for transcriptome analysis

By qRT-PCR, we confirmed the differential mRNA expression of some genes derived from RNA-seq in MC3T3-E1, C2C12, and Ocy454 cell lines using a LightCycler 96 system (Roche Diagnostics, Manheim, Germany). Data were normalized to the levels of and β-actin and glyceraldehyde 3-phosphate dehydrogenase. Relative gene expression levels were calculated using the $2^{(-\Delta\Delta CT)}$ method. The all PCR primer sequences are shown in Table 1.

Table 1. A list of genes and their primer sequences for quantitative real-time polymerase chain reaction

	Forward	**Reverse**
GAPDH	CACAAACTCAGCGGCATAGAAA	GGAAGAGGTAGCCTGCACACAT
β-Actin	ACCCCGTGCTGCTGACCGAG	TCCCGGCCAGCCAGGTCCA
ALP	TCAGGGCAATGAGGTCACATC	CACAATGCCCACGGACTTC
Osteocalcin	CCACCCGGGAGCAGTGT	GAGCTGCTGTGACATCCATACTTG
SOST	GCCTCATCTGCCTACTTGTG	CTGTGGCATCATTCCTGAAG
MyoD	GCTGCTTTTGGCAGATGCACC	GTTTGAGCCTGCAGGACACT
Myogenin	TTCTACCAGGAGCCCCACTT	CCACCGACACAGACTTCCTC
Xirp2 (E7/8)	GTCATCTCTGGCCACATCCT	TGATGGCATCTGAAGCAAGA
AMPD1	TATCAGCATGCAGAGCCTCGCTTA	TGTGGCAGGAAATTCTTGGATCGG
Mettl11b	CTTTCAGAGCTACCTCTACC	GAAATTCACGAGAGGCTTGG

NEXN	CATGCTAGCATATAGCAAACA TGAATGACG	GGGGATCCTAGTAGTCATCCA TTTCAAT
CYP2E1	CGTTGCCTTGCTTGTCTGGA	AAGAAAGGAATTGGGAAAGG TCC
Bche	ACCCAGGGCAATAGCACAAT GTGGC	CTGCCTTCCACTCTTGCTCCG TTTCA
Ppp1r3c	TGCAATGGAAACCTGACGGA	AAGTTCTCCACTCTCCCCCA
Tceal7	ACTTGTGGCCAAGGAGAAGA	GGGTTGTTCATCCTCCCTCT
Gadl1	CGCATTTGACCCCCTGGATG	CGGCGGTGCTTTCTTGACA

Modified from Hong et al. Endocrinol Metab (Seoul) 2020;35:456-469 [25].

Results

Hindlimb unloading-induced bone loss *in vivo*

We measured body weight-adjusted total body BMD and hindlimb BMC with hindlimb unloading and controls by DXA at different time points. At 4 weeks after hindlimb unloading, the total body BMD of mice decreased than that of controls (postnatal week 8) (Figure 5A). In addition, hindlimb BMC was significantly decreased in the left hindlimbs compared to the right hindlimbs (non-unloaded control) at postnatal weeks 9, 10, and 12 (Figure 5B).

Figure 5. Changes in bone mass during mechanical unloading *in vivo*

In vivo measurements of bone mass with dual-energy X-ray absorptiometry. (A) Body weight-adjusted total body bone mineral density (BMD) and (B) hindlimb bone mineral content (BMC). Data are expressed as mean±standard error (n=8–10 per group). [a]P<0.05. Modified from Hong et al. Endocrinol Metab (Seoul) 2020;35:456-469 [25].

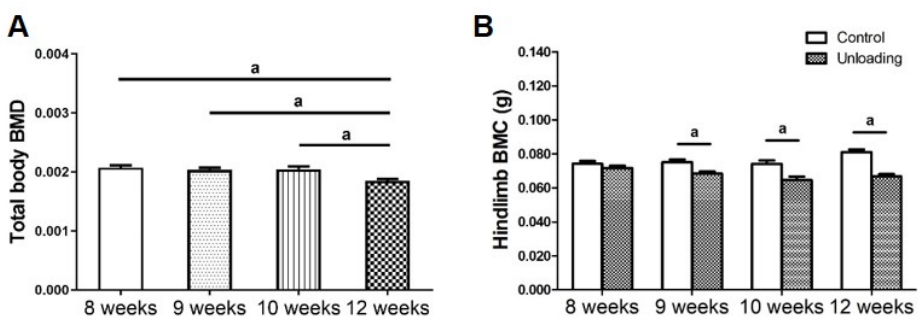

Hindlimb unloading-induced bone loss *ex vivo*

We examined μCT analysis of trabecular bone in the proximal tibiae to examine the changes in bone microarchitecture after hindlimb unloading. Figure 6A depicts representative three-dimensional μCT images from 12-week-old mice (4 weeks after hindlimb unloading). In addition to bone mass, there were significant changes in the trabecular microarchitecture of the proximal tibiae. At 1 week after unloading, BV/TV, Tb.Th, and Tb.N of the left hindlimbs were significantly reduced compared to the right hindlimbs (P=0.001, P=0.014, and P<0.001, respectively; Figure 6B-D). Similar results were observed at 2 and 4 weeks after hindlimb unloading. At the latter time, Tb.Sp increased in the left hindlimbs compared to the right hindlimbs (P=0.007), that was not observed at 1 and 2 weeks after hindlimb unloading (Figure 6E)

Figure 6. Changes in bone microarchitecture during mechanical unloading *ex vivo*

Ex vivo measurements of bone microarchitecture using micro-computed tomography (μCT). (A) Data are three-dimensional μCT images of the trabecular bone of proximal tibiae from 12-week-old mice (4 weeks after unloading). Left: control hindlimb; Right: unloaded hindlimb. (B) Bone volume/total volume (BV/TV) (%), (C) trabecular thickness (Tb.Th), (D) trabecular number (Tb.N), (E) trabecular separation (Tb.Sp). The data are expressed as mean±standard error (n=8–10 per group). [a]P<0.05. Modified from Hong et al. Endocrinol Metab (Seoul) 2020;35:456-469 [25].

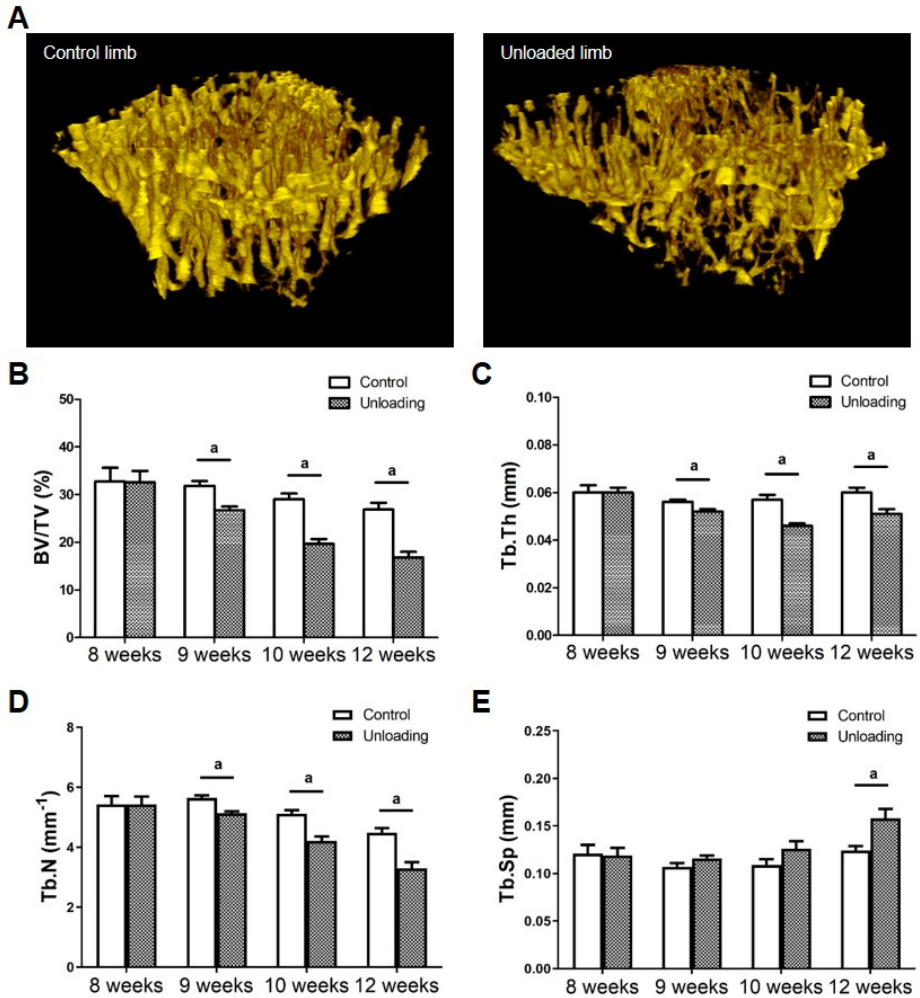

SOST mRNA expression in the femur in response to unloading

There was a significant decrease in *SOST* mRNA expression in the unloaded hindlimbs at postnatal week 9 compared to week 8 (before intervention) (P<0.001; Figure 7). However, the levels of *SOST* mRNA expression did not differ between the unloaded and control hindlimbs or between unloaded hindlimbs.

Figure 7. mRNA expression level of *SOST* in the femur in response to mechanical unloading

Data are expressed as mean±standard error (n=5 per group). [a]P<0.05.

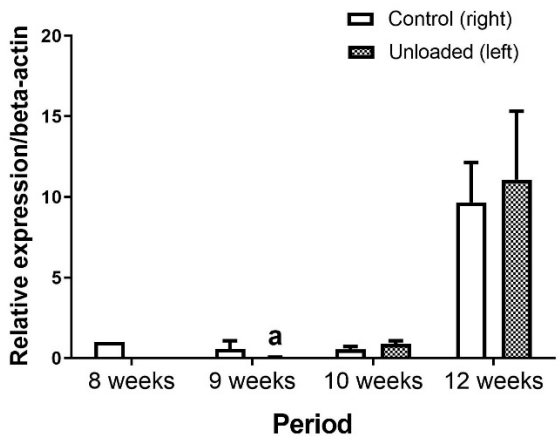

Unilateral hindlimb unloading-induced decreases in serum P1NP levels

To evaluate whether unilateral hindlimb unloading induced changes in serum bone formation marker, we measured P1NP levels in mice at each time point (Figure 8A). Serum P1NP levels were reduced in mice euthanized at postnatal weeks 9 and 12, however increased in those euthanized at postnatal week 10 compared to those euthanized at postnatal week 8 (postnatal week 8: 8.11±0.34 ng/mL; postnatal week 9: 2.94±0.35 ng/mL; postnatal week 10: 10.37±0.88 ng/mL; postnatal week 12: 3.78±0.42 ng/mL; postnatal week 8 vs. 9, P<0.001; postnatal week 8 vs. 10, P=0.067; postnatal week 8 vs. 12, P<0.001; postnatal week 9 vs. 10, P<0.001; postnatal week 9 vs. 12, P=0.177; postnatal week 10 vs. 12, P<0.001).

We also measured the serum levels of bone resorption markers, sclerostin and CTX. Serum levels of bone resorption markers, sclerostin and CTX, were unaffected by unilateral hindlimb unloading (P=0.064 and P=0.061, respectively; Figure 8B and C).

Figure 8. Effects of unloading on serum levels of bone turnover markers

(A) N-terminal propeptide of type I procollagen (P1NP) (B) sclerostin (C) C-telopeptide of type 1 collagen (CTX). Data are presented as mean±standard error (*n*=15 per group). [a]*P*<0.05. Reproduced from Hong et al. Endocrinol Metab (Seoul) 2020;35:456-469 [25].

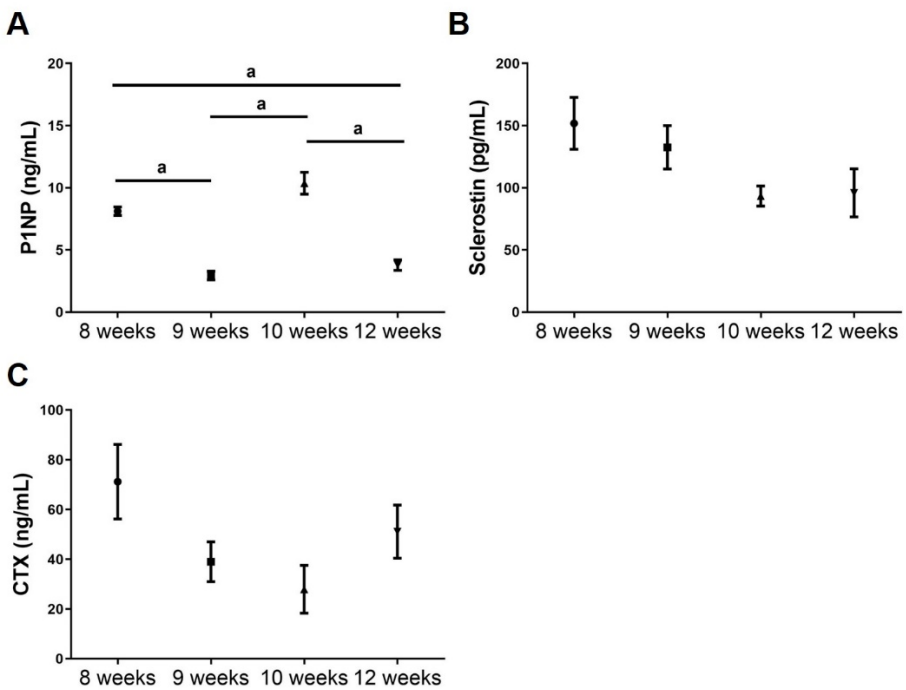

Unloading-induced changes in the number and thickness of X-gal (+) cells on the periosteum of the femur

The 10-kb *Dmp1*-CreERt2 transgene is working in a subset of osteoblasts and osteocytes on the surface of long bones and calvariae [15,16,35]. As mentioned above, 4-OHTam administration induces CreERt2-mediated genetic recombination. This inducible system allows gene labeling of CreERt2-expressing cells at a specific time point since 4-OHTam activity is only detected for 24 hours after injection [36].

For a lineage-tracing study, mice were euthanized at weeks 8 (before intervention), 9, 10, and 12 (Figure 9). Postnatal 8-week-old mice were euthanized 2 days after the last 4-OHTam administration. At postnatal week 8, many labeled osteoblasts and osteocytes were observed on the periosteal surface of the femur by X-gal staining (Figure 9A). At postnatal week 12 (4 weeks after the last 4-OHTam), X-gal (+) cells were barely visible on the periosteum of the femur (Figure 9A). The number and thickness of X-gal (+) osteoblastic descendants were quantified at postnatal weeks 8, 9, 10, and 12 (i.e., 2 days, 1 week, 2 weeks, and 4 weeks after the last 4-OHTam) and compared between the left hindlimbs and right hindlimbs (non-unloaded control). At 1 week after unloading (postnatal week 9), the number (right: 15.5±2.2/mm; left: 9.6±1.4/mm; P=0.790) and thickness (right: 2.7±0.2 μm; left: 2.4±0.3 μm; P=0.273) of X-gal (+) cells did not differ between the left hindlimbs and right hindlimbs (Figure 9B and C). However, at 2 weeks after unloading (postnatal week 10), the number of X-gal (+) cells significantly decreased in the left hindlimbs (right: 10.9±0.8/mm; left: 7.3±2.4/mm; P=0.038). In addition, a subtle change in the thickness of X-gal (+) cells (right: 3.5±0.2 μm; left: 2.9±0.2 μm; P=0.071) was observed in the left compared to the right hindlimbs (Figure 9B and C). At 4 weeks after unloading (postnatal week 12), the decrease in thickness of X-gal (+) cells was greater in the left compared to the right hindlimbs (right: 2.7±0.2 μm; left: 2.0±0.3 μm; P=0.030). While, the number of X-gal (+) cells was comparable on both hindlimbs (right: 9.3±1.9/mm; left: 8.1±1.1/mm; P=0.760) (Figure 9B and C).

Figure 9. **Effects of unloading on the conversion of active mature osteoblasts to bone lining cells on the periosteum of the femur**

X-gal staining was conducted in both hindlimbs on postnatal 8, 9, 10, and 12 weeks (i.e., 2 days, 1 week, 2 weeks, and 4 weeks after the last 4-hydroxy-tamoxifen, respectively). Mechanical unloading was done on the left hindlimbs and the right hindlimbs was considered as controls. (A) Data are representative of the experiments performed in the sections. Quantitative analysis of the (B) number and (C) thickness of X-gal (+) cells on the periosteum of the femur. Data are expressed as mean± standard error (n=4–6 per group). [a]P<0.05 between control hindlimbs; [b]P<0.05 between unloaded hindlimbs; [c]P<0.05 between the unloaded and control hindlimbs at each time point. Adapted from Hong et al. Endocrinol Metab (Seoul) 2020;35:456-469 [25].

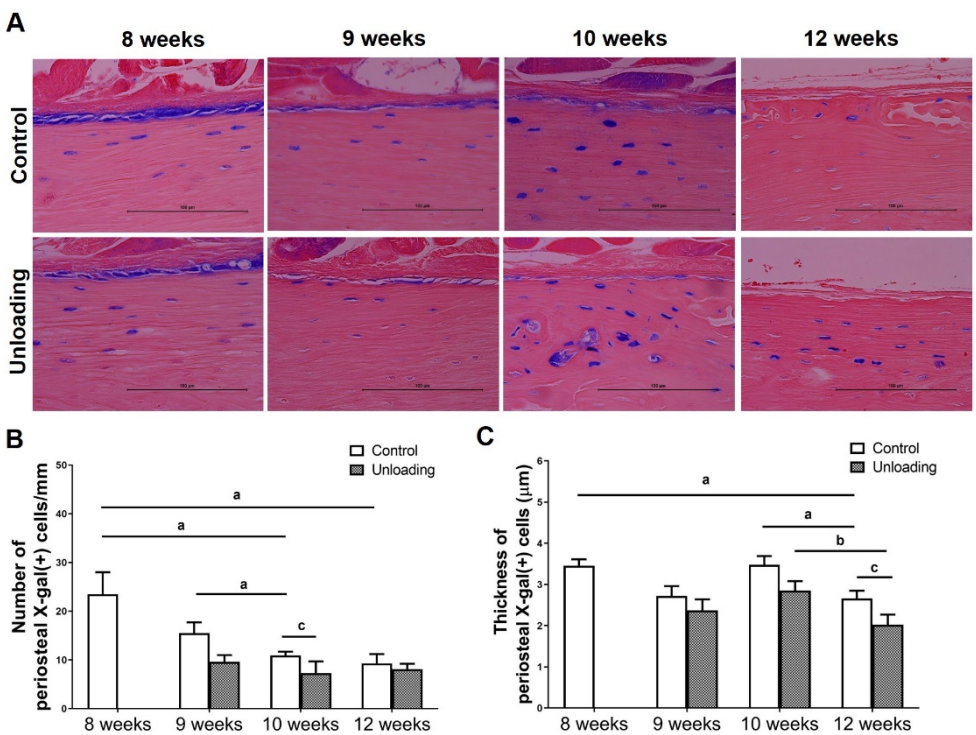

DEG analysis

Analysis of the postnatal weeks 10 and 12 datasets revealed 3211 DEGs (Figure 10). At postnatal week 10, 99 genes were upregulated and 1,364 were downregulated, and at postnatal week 12, 1,001 were upregulated and 1,091 were downregulated (Figure 10A and B). We integrated the two datasets and split the DEGs into up-up, up-down, down-up, and down-down (for illustration, continuously upregulated gene in both datasets was classified as “up-up”; continuously downregulated gene in both datasets was classified as “down-down”). As shown in the Venn diagram (Figure 10C), there were 5 up-up, 315 down-down, 7 up-down, and 17 down-up genes.

In PCA of the femur gene expression pattern, we observed a high correlation between the unloaded and control limbs at each time point, indicating low heterogeneity of the analyzed samples (Figure 4).

Figure 10. Scatter plot of log_2 fold changes and Venn diagram for differentially expressed gene analysis

RNA seq-based transcriptome analysis for differentially expressed genes (DEGs) after mechanical unloading in mice euthanized at postnatal weeks 10 and 12. Log_2 fold changes (FCs) were calculated for all genes of each mouse. DEGs were defined based on the following criteria: (1) $|log_2(FC)|>log_2(1.2)$ and $|avg(log_2(FC)|>log_2(1.5)$ at weeks 8 and 12 and (2) each $log_2(FC)>log_2(1.5)$ at week 10. Scatter plot of DEG analysis at postnatal weeks (A) 10 and (B) 12. Red circles: upregulated (Up) DEGs, blue circles: downregulated (Dn) DEGs, and gray circles: non-DEGs. (C) Venn diagram for DEG analysis. Each number is the number of up- and downregulated

genes at postnatal weeks 10 and 12 (*n*=3/group at weeks 8 and 12; *n*=2/group at week 10). By courtesy of Kwangsoo Kim. Adapted from Hong et al. Endocrinol Metab (Seoul) 2020;35:456-469 [25].

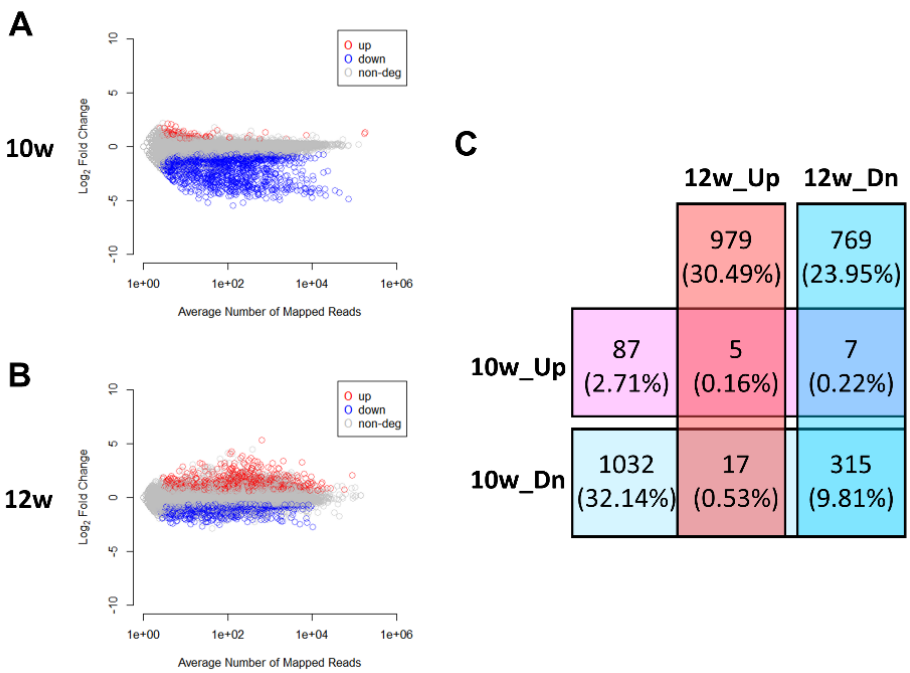

DAVID-based gene set analysis and PPI network analysis

A gene set analysis of the 315 down-down regulated genes was performed using DAVID (Figure 11). Individual analysis of gene sets in terms of biological processes, cellular component, molecular function, and Kegg pathway revealed that several genes, including those involved in muscle contraction, glucose metabolism, and calcium signaling, were identified to be significantly affected by unloading.

Figure 11. Gene set analysis for 315 down-down regulated genes at postnatal weeks 10 and 12 using DAVID web-based tool

P values were generated from the fisher's exact test. Significantly enriched gene sets were obtained by a Benjamini-Hochberg adjusted *P* value (*q* value) <0.05. By courtesy of Kwangsoo Kim. Adapted from Hong et al. Endocrinol Metab (Seoul) 2020;35:456-469 [25].

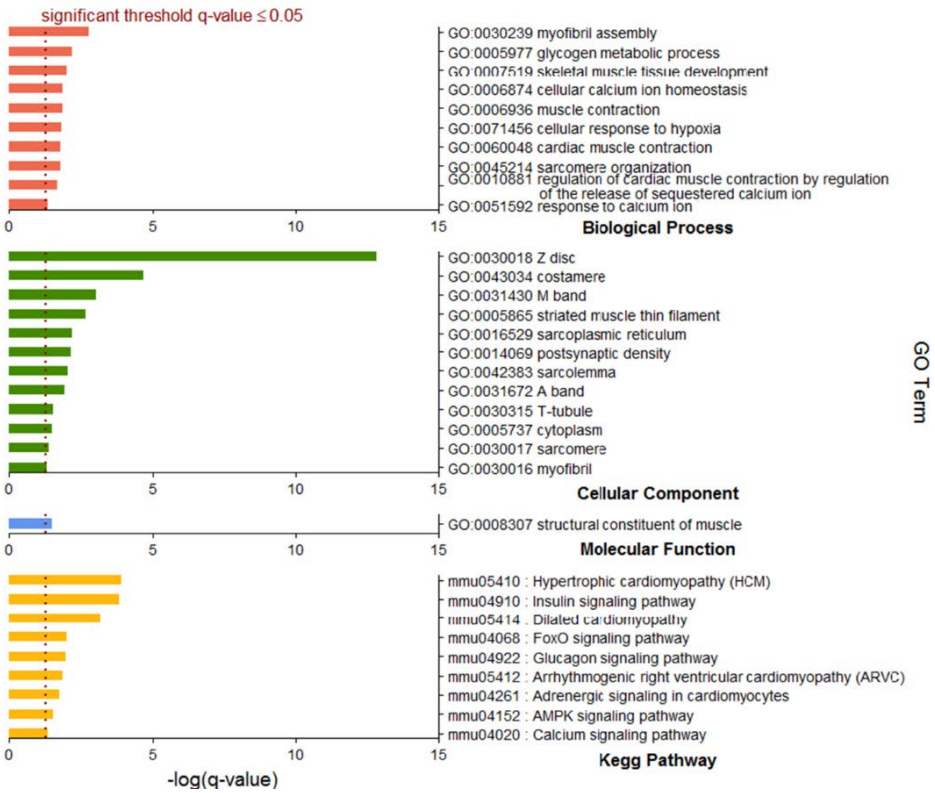

We built a final PPI network with 216 nodes and 552 edges (the average node degree of 5.111 and average local clustering coefficient of 0.223). The EAGLE algorithm discovered a total of 7 subnetworks, in which subnetwork 1 showed the highest modularity (modularity of 6.795). In subnetwork 1 having 56 nodes and 299 edges, four major down-down regulated DEGs were identified including *AMPD1*, *Bche*, *NEXN*, and *Xirp2* (Figure 12).

Figure 12. Protein-protein interaction network analysis for differentially expressed genes in subnetwork 1

For the analysis of the protein-protein interaction network, the STRING database was used based on the proteins corresponding to selected DEGs. By courtesy of Kwangsoo Kim. Adapted from Hong et al. Endocrinol Metab (Seoul) 2020;35:456-469 [25].

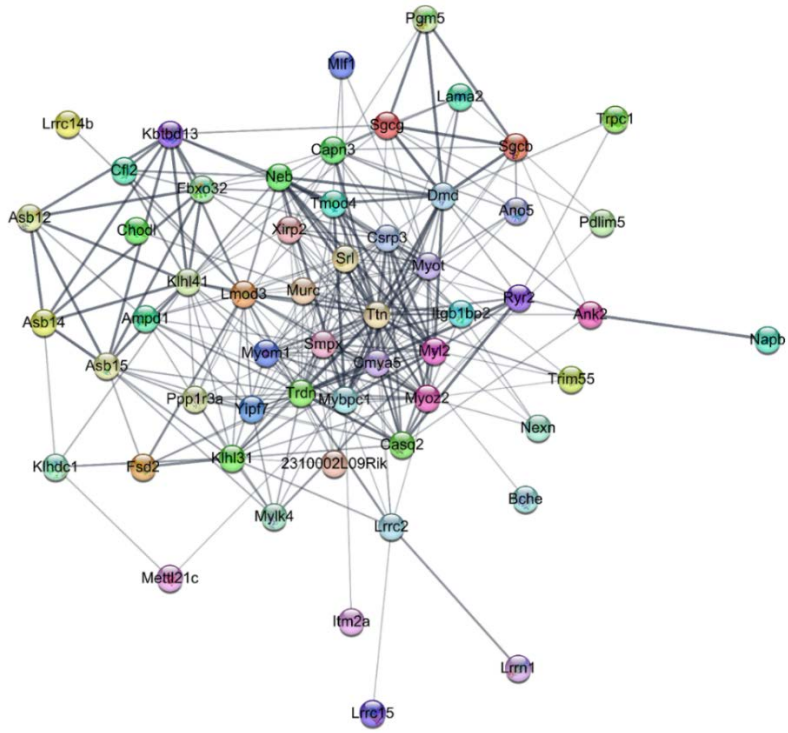

In subnetwork 1, CluePedia-based network expansion of 56 genes found an additional 47 neighboring genes, for a total of 103 genes used for the gene set analysis. The gene set analysis discovered potential interactions between DEGs, such as calcium signaling and glucose metabolism, that were similar to the results from the DAVID analysis (Table 2).

Table 2. A list of gene set analysis using the Cytoscape ClueGO app for subnetwork 1 from the whole protein-protein interaction network

Gene ontology			
(A) Biological process			
GO ID	GO Term	*P*-value	*q*-value
GO:0030239	Myofibril assembly	7.13836e-32	2.14151e-30
GO:0055001	Muscle cell development	9.77759e-31	2.28144e-29
GO:0010927	Cellular component assembly involved in morphogenesis	1.8542e-30	3.89383e-29
GO:0055002	Striated muscle cell development	5.23465e-30	9.99342e-29
GO:0003012	Muscle system process	3.45239e-29	6.04168e-28
GO:0051146	Striated muscle cell differentiation	1.18493e-25	1.91411e-24
GO:0042692	Muscle cell differentiation	2.45594e-24	3.68391e-23
GO:0031032	Actomyosin structure organization	1.63891e-23	2.29448e-22
GO:0061061	Muscle structure development	2.607e-22	3.42169e-21
GO:0045214	Sarcomere organization	3.28874e-21	3.83687e-20
GO:0014706	Striated muscle tissue development	1.2991e-20	1.43584e-19
GO:0060537	Muscle tissue development	3.74621e-20	3.93353e-19
(B) Cellular component			
GO ID	GO Term	*P*-value	*q*-value
GO:0030016	Myofibril	7.06676e-55	1.48402e-52
GO:0044449	Contractile fiber part	6.9926e-54	4.89482e-52
GO:0043292	Contractile fiber	4.76476e-54	4.89482e-52
GO:0030017	Sarcomere	5.53863e-53	2.90778e-51
GO:0031674	I band	5.57587e-38	2.34187e-36
GO:0030018	Z disc	2.45447e-37	8.59064e-36
GO:0099512	Supramolecular fiber	4.1822e-31	1.09783e-29
GO:0031672	A band	1.82973e-21	2.26025e-20
GO:0016529	Sarcoplasmic reticulum	3.92812e-19	3.74957e-18
GO:0016528	Sarcoplasm	3.62202e-18	3.16927e-17
GO:0033017	Sarcoplasmic reticulum membrane	5.0388e-16	3.20651e-15
GO:0031430	M band	2.5026e-14	1.33584e-13
(C) Molecular function			
GO ID	GO Term	*P*-value	*q*-value
GO:0003779	Actin binding	2.58389e-16	1.75037e-15
GO:0042805	Actinin binding	1.52331e-12	6.03577e-12
GO:0051015	Actin filament binding	3.12904e-11	1.02672e-10
GO:0051393	Alpha-actinin binding	4.28915e-10	1.251e-09
GO:0044325	Ion channel binding	2.56145e-08	5.66214e-08
GO:0017166	Vinculin binding	4.2601e-07	7.84755e-07
GO:0051371	Muscle alpha-actinin binding	1.00207e-06	1.69706e-06
GO:0031433	Telethonin binding	5.37821e-06	8.06732e-06

GO:0005523	Tropomyosin binding	2.70059e-05	3.73108e-05
GO:0005080	Protein kinase C binding	0.000395349	0.000466423
GO:0017022	Myosin binding	0.000416141	0.000485498
GO:0048306	Calcium-dependent protein binding	0.000460048	0.000530825
Kegg pathway			
Kegg ID	Kegg pathway name	*P*-value	*q*-value
KEGG:05410	Hypertrophic cardiomyopathy	6.08427e-15	3.54916e-14
KEGG:05414	Dilated cardiomyopathy	1.07342e-14	5.93205e-14
KEGG:05412	Arrhythmogenic right ventricular cardiomyopathy	1.55384e-09	4.2935e-09
KEGG:05416	Viral myocarditis	7.84991e-09	1.87327e-08
KEGG:04510	Focal adhesion	4.22917e-06	6.43569e-06
KEGG:04022	cGMP-PKG signaling pathway	1.59648e-05	2.25007e-05
KEGG:04611	Platelet activation	0.000297419	0.000361029
KEGG:04260	Cardiac muscle contraction	0.000483196	0.000551474
KEGG:04911	Insulin secretion	0.000699202	0.000781024

In gene ontology analysis, top 12 GO IDs were presented in each category based on *q*-value. Reproduced from Hong et al. Endocrinol Metab (Seoul) 2020;35:456-469 [25].

Evaluation of mRNA expression levels of down-down regulated genes during osteoblastogenic, osteocytic, and myogenic differentiation

Among the 315 down-down regulated genes, nine genes that had high FC values and were regarded to have biological functions implicated to bone and muscle (i.e., *Xirp2, AMPD1, NEXN, CYP2E1, Bche, Mettl11b, Ppp1r3c, Gadl1,* and *Tceal7*). We performed qRT-PCR to confirm the mRNA expression levels of these genes in MC3T3-E1 and C2C12 cells. The mRNA expression of all nine genes was upregulated during osteoblastogenic and myogenic differentiation (Figure 13A and B). Since osteocytes comprise the majority of cells obtained from femur specimens, *SOST*-expressing Ocy454 osteocytic cells were used to further confirm the mRNA expression levels of above genes during osteocytic differentiation [37]. Significantly increased levels of *Xirp2, AMPD1, Mettl11b, Ppp1r3c, Gadl1,* and *Tceal7* were observed during osteocytic differentiation (Figure 13C).

Figure 13. mRNA expression levels of nine genes continuously downregulated at postnatal weeks 10 and 12 during the differentiation of (A) MC3T3-E1, (B) C2C12, and (C) Ocy454 cell line using quantitative RT-PCR

Data were normalized to the levels of and β-actin and glyceraldehyde 3-phosphate dehydrogenase. [a]P<0.05 between undifferentiated and differentiated cell lines. Adapted from Hong et al. Endocrinol Metab (Seoul) 2020;35:456-469 [25].

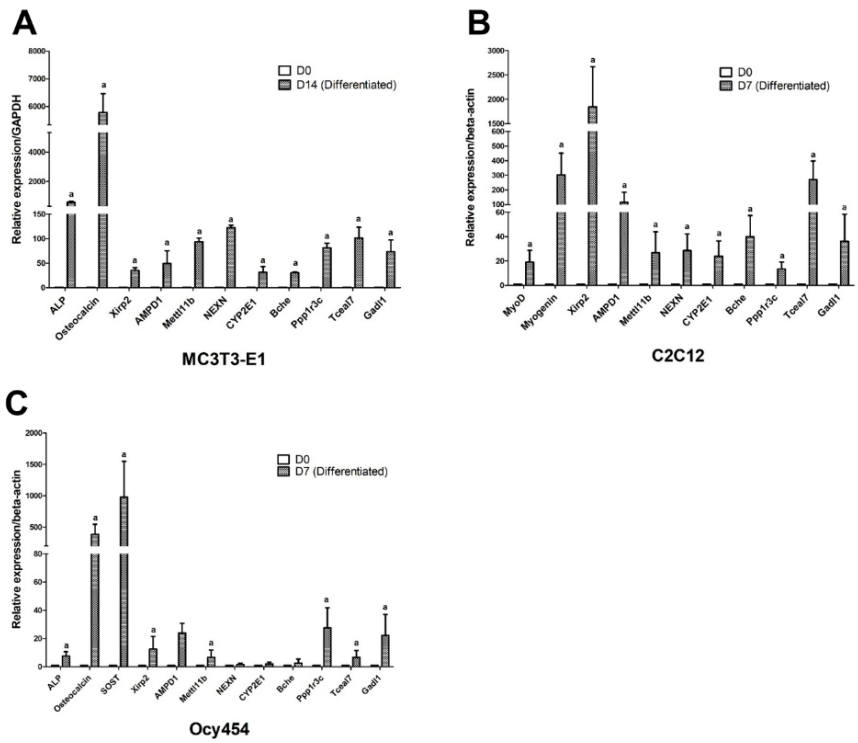

Discussion

The present study provides direct evidence of the effect of mechanical unloading on the fate of mature active osteoblasts that differentiate into BLCs. Unloading accelerated this process in the opposite direction of intermittent PTH or sclerostin antibody treatment. Furthermore, RNA-seq data showed that mechanical unloading resulted in significant changes in the transcriptome profile after the unloading period compared to non-unloaded control. We identified 315 DEGs that were continuously down-regulated during unloading. Notably, the mRNA expression of *AMPD1, Xirp2, Mettl11b, NEXN, CYP2E1, Bche, Gadl1, Tceal7,* and *Ppp1r3c* increased in differentiated osteoblast/osteocytic as well as myoblast cell lines.

Two independent approaches (lineage tracing study and RNA-seq-based transcriptome profiling) were used to investigate the cellular and molecular mechanisms of mechanical unloading-induced bone loss. A combination of botulinum toxin injection and Achilles tenotomy was used to achieve unilateral hindlimb unloading in mice and induce bone loss *in vivo*. Mature osteoblasts remain on the bone surface as inactive BLCs or are implanted in the bone matrix as osteocytes. Previously reported lineage-tracing studies have shown that the majority of X-gal (+) cells (i.e., mature active osteoblasts) were cuboidal and plump at 2 days after the last 4-OHTam treatment on the periosteal surface [15-17]. However, they were converted to quiescent BLCs and flattened, resulting in almost invisible on the bone surface over time. Using a lineage-tracing model, a significant decrease in the number of X-gal (+) cells on the periosteum of unloaded limb at 2 weeks, and a decrease in the thickness of those cells at 4 weeks after unloading was observed compared to non-unloaded control. These results indicate that mechanical unloading

accelerates the conversion of active mature osteoblasts to quiescent BLCs *in vivo*. In addition, a significant decrease in serum P1NP levels after unloading was observed, indicating a decrease in bone formation. These findings provide the first evidence that mechanical unloading affects BLCs. Specifically, it is the opposite of mechanical loading. It is difficult to explain the rise in P1NP levels at week 10. Adding to the botulinum toxin injections at postnatal weeks 8 and 10, an Achilles tenotomy was performed on the left hindlimb to induce unloading at week 9. This procedure may have resulted in greater bone loss than that occurred in response to botulinum toxin injection, thereby stimulating the compensatory mechanism of the contralateral limb and associated with increased P1NP levels. Our study did not assess the number of osteocytes (either total osteocytes or X-gal+ osteocytes), proliferation, and apoptosis of osteoblast lineage cells in response to mechanical unloading. In previous studies, intermittent PTH or sclerostin antibody did not affect the number of X-gal (+) osteocytes in long bones [15,17].

To elucidate the molecular mechanisms underlying mechanical unloading-induced bone loss, we examined transcriptome profiles obtained using the same unloading protocol as in the lineage-tracing study. There is a possibility that contamination by tissues, which have a high cell/matrix ratio (e.g., bone marrow or muscle), can elicit variations in gene expression patterns, and the degree of such contamination is individual. To minimize the effects of contamination, we determined the time sequence of the same mouse-paired bone DEGs, in which the left hindlimb was unloaded and the right hindlimb served as a control. The PCA of the femur gene expression pattern (Figure 4) showed low heterogeneity in the sample between the unloaded femurs and the control femurs. Since the ultimate outcome of

this study was not absolute gene expression levels at each time, but relative changes in DEGs between unloaded and control hindlimbs over time, the results of RNA-seq analysis are reliable.

In the present study, DEGs between unloaded and control limbs were analyzed at 2 and 4 weeks following unloading. Changes in gene expression patterns occur indeed before changes in bone phenotypes. Therefore, our experiments could not represent early responses after unloading, and it is possible that a combination of delayed response and induction of certain compensatory mechanisms may have affected our data. In addition, hindlimb unloading was achieved by repeating the procedure at weekly intervals rather than a single procedure, which can complicate the interpretation of the findings. Given these limitations of the study, we focused on gene sets showing similar expression trends (e.g., down-down or up-up) at 2 and 4 weeks after mechanical unloading. Indeed, most genes showed the down-down pattern during unloading.

We reviewed the gene expression atlases of the European Bioinformatics Institute (www.ebi.ac.uk) and the Mouse Genome Database (www.informatics.jax.org) to find pleiotropic genes that may have biological functions in both bone and muscle. Among genes highly expressed in bone and muscle, genes that are abundantly expressed in other tissues were excluded. We also reviewed RNA-seq data previously published by Ayturk et al. [38] from the tibia, bone marrow, and muscle of 10-week-old mice. They did not exactly match our own data, but they were a useful reference to narrow down the number of candidate genes we searched for.

Finally, the following nine genes were selected for *in vitro* validation by qRT-PCR and shown to be upregulated during osteoblastogenic/osteocytic and

myogenic differentiation. *Xirp2* (encoding Xin-actin binding repeat containing 2), *Mettl11b* (methyl transferase-like protein 11b), *NEXN* (nexilin, F-actin binding protein), *AMPD1* (adenosine monophosphate deaminase 1), *Tceal7* (transcription elongation factor A like 7), *Ppp1r3c* (protein phosphatase 1 regulatory subunit 3c), *CYP2E1* (cytochrome P450 2E1), *Bche* (butyrylcholinesterase), and *Gadl1* (glutamate decarboxylase-like protein 1). *Xirp2* is expressed in skeletal and cardiac muscle, and a hypomorphic *Xirp2* allele is related to cardiac hypertrophy [39]. Mutations in *NEXN* have been associated with hypertrophic cardiomyopathy [40]. *CYP2E1* induces oxidative stress and impairs insulin action [41]. Similarly, *Ppp1r3c* regulates glycogen metabolism, in particular, glycogen synthesis [42]. *AMPD1* is involved in the regulation of glucose metabolism by regulating the activation of AMP-activated protein kinase in muscle, and *AMPD1* deficiency contributes to improved insulin resistance [43]. *Tceal7* encodes an ovarian tumor suppressor which suppresses myoblast proliferation and promotes the myoblast differentiation into myotubes [44]. *Bche*, which can cleave acetylcholine, is detected in MC3T3-E1 cells and may regulate bone cell-matrix interactions by inducing acethylcholine degradation in early stages of osteoblast differentiation [45]. The biological functions of *Mettl11b* and *Gadl1* have not yet been determined.

Mechanical loading increases bone formation, in which canonical Wnt signaling pathway plays a major role [46]. Sclerostin, which is encoded by the *SOST* gene and secreted by osteocytes, is an endogenous Wnt signaling antagonist that is downregulated during mechanical loading [47,48], although this varies according to the bone region [49-51]. In our study, *SOST* expression levels in the femur diaphysis did not differ between mice with and without unloading in by RNA-seq and qRT-

PCR analysis. We also observed no changes in serum sclerostin level during unloading. This may be attributed to the different time intervals after unloading and bone regions analyzed compared to previous reports. It is also possible that there is a compensatory response from contralateral non-unloaded limbs that may indirectly experience increased loading. The net effect of loading and unloading on different hindlimbs may lead to no significant changes in serum levels of bone resorption markers including sclerostin.

It remains unclear how unloading affects the changes in gene expression profiles of active mature osteoblasts, leading to rapid differentiation of these cells to quiescent BLCs. To perform single cell sequencing is the best way to compare transcriptome profiling between inactive BLCs and active mature osteoblasts. However, it is currently very difficult to isolate BLCs and active mature osteoblasts *in vivo*. Therefore, it is not possible to confirm that the gene sets affected mechanical unloading are similar to those of active mature osteoblasts and osteocytes. Future studies are needed to elucidate this issue.

In conclusion, the present findings suggest possible cellular mechanisms for mechanical unloading-induced bone loss and provide gene sets to dissect the regulatory network that governs this process. The identified genes can exert pleiotropic effects on bone and muscle.

References

1. Lanyon LE, Hampson WG, Goodship AE, Shah JS. Bone deformation recorded in vivo from strain gauges attached to the human tibial shaft. *Acta Orthop Scand* 1975;46:256-68.

2. Usui T, Maki K, Toki Y, Shibasaki Y, Takanobu H, Takanishi A, et al. Measurement of mechanical strain on mandibular surface with mastication robot: influence of muscle loading direction and magnitude. *Orthod Craniofac Res* 2003;6 Suppl 1:163-7,179-82.

3. Hong AR, Kim SW. Effects of resistance exercise on bone health. *Endocrinol Metab (Seoul)* 2018;33:435-44.

4. Globus RK, Bikle DD, Morey-Holton E. The temporal response of bone to unloading. *Endocrinology* 1986;118:733-42.

5. Vandamme K, Holy X, Bensidhoum M, Deschepper M, Logeart-Avramoglou D, Naert I, et al. Impaired osteoblastogenesis potential of progenitor cells in skeletal unloading is associated with alterations in angiogenic and energy metabolism profile. *Biomed Mater Eng* 2012;22:219-26.

6. Inoue M, Tanaka H, Moriwake T, Oka M, Sekiguchi C, Seino Y. Altered biochemical markers of bone turnover in humans during 120 days of bed rest. *Bone* 2000;26:281-6.

7. Vico L, Collet P, Guignandon A, Lafage-Proust MH, Thomas T, Rehaillia M, et al. Effects of long-term microgravity exposure on cancellous and cortical weight-bearing bones of cosmonauts. *Lancet* 2000;355:1607-11.

8. LeBlanc A, Marsh C, Evans H, Johnson P, Schneider V, Jhingran S. Bone and muscle atrophy with suspension of the rat. *J Appl Physiol (1985)* 1985;58:1669-75.

9. Fitts RH, Metzger JM, Riley DA, Unsworth BR. Models of disuse: a comparison of hindlimb suspension and immobilization. *J Appl Physiol (1985)* 1986;60:1946-53.

10. Judex S, Garman R, Squire M, Busa B, Donahue LR, Rubin C. Genetically linked site-specificity of disuse osteoporosis. *J Bone Miner Res* 2004;19:607-13.

11. Doherty TJ. The influence of aging and sex on skeletal muscle mass and strength. *Curr Opin Clin Nutr Metab Care* 2001;4:503-8.

12. Palmer IJ, Runnels ED, Bemben MG, Bemben DA. Muscle-bone interactions across age in men. *J Sports Sci Med* 2006;5:43-51.

13. Raisz LG, Seeman E. Causes of age-related bone loss and bone fragility: an alternative view. *J Bone Miner Res* 2001;16:1948-52.

14. Raisz LG, Rodan GA. Pathogenesis of osteoporosis. *Endocrinol Metab Clin North Am* 2003;32:15-24.

15. Kim SW, Pajevic PD, Selig M, Barry KJ, Yang JY, Shin CS, et al. Intermittent parathyroid hormone administration converts quiescent lining cells to active osteoblasts. *J Bone Miner Res* 2012;27:2075-84.

16. Jang MG, Lee JY, Yang JY, Park H, Kim JH, Kim JE, et al. Intermittent PTH treatment can delay the transformation of mature osteoblasts into lining cells on the periosteal surfaces. *J Bone Miner Metab* 2016;34:532-9.

17. Kim SW, Lu Y, Williams EA, Lai F, Lee JY, Enishi T, et al. Sclerostin antibody administration converts bone lining cells into active osteoblasts. *J Bone Miner Res* 2017;32:892-901.

18. Boppart MD, Kimmel DB, Yee JA, Cullen DM. Time course of osteoblast appearance after in vivo mechanical loading. *Bone* 1998;23:409-15.

19. Dallas SL, Prideaux M, Bonewald LF. The osteocyte: an endocrine cell ... and

more. *Endocr Rev* 2013;34:658-90.

20. Pedersen BK. Muscle as a secretory organ. Compr Physiol 2013;3:1337-62.

21. Brotto M, Bonewald L. Bone and muscle: interactions beyond mechanical. *Bone* 2015;80:109-14.

22. Kramer I, Baertschi S, Halleux C, Keller H, Kneissel M. Mef2c deletion in osteocytes results in increased bone mass. *J Bone Miner Res* 2012;27:360-73.

23. Huang J, Hsu YH, Mo C, Abreu E, Kiel DP, Bonewald LF, et al. METTL21C is a potential pleiotropic gene for osteoporosis and sarcopenia acting through the modulation of the NF-κB signaling pathway. *J Bone Miner Res* 2014;29:1531-40.

24. Soriano P. Generalized lacZ expression with the ROSA26 Cre reporter strain. *Nat Genet* 1999;21:70-1.

25. Hong AR, Kim K, Lee JY, Yang JY, Kim JH, Shin CS et al. Transformation of Mature Osteoblasts into Bone Lining Cells and RNA Sequencing-Based Transcriptome Profiling of Mouse Bone during Mechanical Unloading. *Endocrinol Metab (Seoul)* 2020;35:456-69.

26. Chung UI, Lanske B, Lee K, Li E, Kronenberg H. The parathyroid hormone/parathyroid hormone-related peptide receptor coordinates endochondral bone development by directly controlling chondrocyte differentiation. *Proc Natl Acad Sci U S A* 1998;95:13030-5.

27. Bolger AM, Lohse M, Usadel B. Trimmomatic: a flexible trimmer for Illumina sequence data. *Bioinformatics* 2014;30:2114-20.

28. Dobin A, Davis CA, Schlesinger F, Drenkow J, Zaleski C, Jha S, et al. STAR: ultrafast universal RNA-seq aligner. *Bioinformatics* 2013;29:15-21.

29. Liao Y, Smyth GK, Shi W. FeatureCounts: an efficient general purpose program

for assigning sequence reads to genomic features. *Bioinformatics* 2014;30:923-30.

30. Dennis G Jr, Sherman BT, Hosack DA, Yang J, Gao W, Lane HC, et al. DAVID: database for annotation, visualization, and integrated discovery. *Genome Biol* 2003;4:P3.

31. Doncheva NT, Morris JH, Gorodkin J, Jensen LJ. Cytoscape StringApp: network analysis and visualization of proteomics data. *J Proteome Res* 2019;18:623-32.

32. Wang J, Zhong J, Chen G, Li M, Wu FX, Pan Y. ClusterViz: a Cytoscape app for cluster analysis of biological network. *IEEE/ACM Trans Comput Biol Bioinform* 2015;12:815-22.

33. Bindea G, Galon J, Mlecnik B. CluePedia Cytoscape plugin: pathway insights using integrated experimental and in silico data. *Bioinformatics* 2013;29:661-3.

34. Bindea G, Mlecnik B, Hackl H, Charoentong P, Tosolini M, Kirilovsky A, et al. ClueGO: a Cytoscape plug-in to decipher functionally grouped gene ontology and pathway annotation networks. *Bioinformatics* 2009;25:1091-3.

35. Powell WF Jr, Barry KJ, Tulum I, Kobayashi T, Harris SE, Bringhurst FR, et al. Targeted ablation of the PTH/PTHrP receptor in osteocytes impairs bone structure and homeostatic calcemic responses. *J Endocrinol* 2011;209:21-32.

36. Maes C, Kobayashi T, Selig MK, Torrekens S, Roth SI, Mackem S, et al. Osteoblast precursors, but not mature osteoblasts, move into developing and fractured bones along with invading blood vessels. *Dev Cell* 2010;19:329-44.

37. Wein MN, Spatz J, Nishimori S, Doench J, Root D, Babij P, et al. HDAC5 controls MEF2C-driven sclerostin expression in osteocytes. *J Bone Miner Res* 2015;30:400-11.

38. Ayturk UM, Jacobsen CM, Christodoulou DC, Gorham J, Seidman JG, Seidman

CE, et al. An RNA-seq protocol to identify mRNA expression changes in mouse diaphyseal bone: applications in mice with bone property altering Lrp5 mutations. *J Bone Miner Res* 2013;28:2081-93.

39. McCalmon SA, Desjardins DM, Ahmad S, Davidoff KS, Snyder CM, Sato K, et al. Modulation of angiotensin II-mediated cardiac remodeling by the MEF2A target gene Xirp2. *Circ Res* 2010;106:952-60.

40. Wang H, Li Z, Wang J, Sun K, Cui Q, Song L, et al. Mutations in NEXN, a Z-disc gene, are associated with hypertrophic cardiomyopathy. *Am J Hum Genet* 2010;87:687-93.

41. Armoni M, Harel C, Ramdas M, Karnieli E. CYP2E1 impairs GLUT4 gene expression and function: NRF2 as a possible mediator. *Horm Metab Res* 2014;46:477-83.

42. Lee SK, Moon JW, Lee YW, Lee JO, Kim SJ, Kim N, et al. The effect of high glucose levels on the hypermethylation of protein phosphatase 1 regulatory subunit 3C (PPP1R3C) gene in colorectal cancer. *J Genet* 2015;94:75-85.

43. Cheng J, Morisaki H, Toyama K, Sugimoto N, Shintani T, Tandelilin A, et al. AMPD1: a novel therapeutic target for reversing insulin resistance. *BMC Endocr Disord* 2014;14:96.

44. Shi X, Garry DJ. Myogenic regulatory factors transactivate the Tceal7 gene and modulate muscle differentiation. *Biochem J* 2010;428:213-21.

45. En-Nosse M, Hartmann S, Trinkaus K, Alt V, Stigler B, Heiss C, et al. Expression of non-neuronal cholinergic system in osteoblast-like cells and its involvement in osteogenesis. *Cell Tissue Res* 2009;338:203-15.

46. Robinson JA, Chatterjee-Kishore M, Yaworsky PJ, Cullen DM, Zhao W, Li C et

al. Wnt/beta-catenin signaling is a normal physiological response to mechanical loading in bone. *J Biol Chem* 2006;281:31720-8.

47. Robling AG, Niziolek PJ, Baldridge LA, Condon KW, Allen MR, Alam I et al. Mechanical stimulation of bone in vivo reduces osteocyte expression of Sost/sclerostin. *J Biol Chem* 2008;283:5866-75.

48. Mantila Roosa SM, Liu Y, Turner CH. Gene expression patterns in bone following mechanical loading. *J Bone Miner Res* 2011;26:100-12.

49. Macias BR, Aspenberg P, Agholme F. Paradoxical Sost gene expression response to mechanical unloading in metaphyseal bone. *Bone* 2013;53:515-9.

50. Moustafa A, Sugiyama T, Prasad J, Zaman G, Gross TS, Lanyon LE et al. Mechanical loading-related changes in osteocyte sclerostin expression in mice are more closely associated with the subsequent osteogenic response than the peak strains engendered. *Osteoporos Int* 2012;23:1225-34.

51. Sun X, Yang K, Wang C, Cao S, Merritt M, Hu Y et al. Paradoxical response to mechanical unloading in bone loss, microarchitecture, and bone turnover markers. *Int J Med Sci* 2015;12:270-9.

국문초록

배경 및 목적: 기계적 무부하가 골손실을 초래하는 세포학적, 분자학적 기전은 아직 명확히 밝혀지지 않았다. 이에 본 연구에서는 조골세포 계열 추적 연구를 통해 기계적 무부하가 성숙 조골세포를 골표면세포로 전환시키는 과정에서 어떤 역할을 하는 지 쥐 생체 내에서 관찰하고, 동시에 RNA 시퀀싱을 기반으로 한 유전자 발현 양상을 분석하여 기계적 무부하가 골손실에 미치는 영향에 대해 깊이 이해하고자 하였다.

방법: *Dmp1*-CreERt2(+):Rosa26R 7주령 쥐에 1 mg의 타목시펜을 주3회 투여하고, 생후 8주부터 10주까지 왼쪽 뒷다리에 보톡스 주사와 아킬레스 건절개를 시행하여 기계적 무부하를 유도하였다. 생후 8, 9, 10, 12주령에 쥐를 희생한 후 각 시점에 양쪽 대퇴골의 골막에서 X-gal 표지 세포의 수와 두께를 측정하여 표지된 조골세포의 운명을 추적하였다. 동일한 실험 방법 하에 정상 쥐에서 각 시점 별로 대퇴골 골간에서 추출한 RNA를 이용하여 유전자 발현 양상을 분석하였다.

결과: 기계적 무부하 후 1주부터 4주째까지 현저한 대퇴골 질량의 감소가 확인되었다. 무부하 2주 후, 오른쪽에 비해 무부하가 행해진 왼쪽 뒷다리에서 유의미한 X-gal 표지 세포의 수적 감소 및 약간의 두께 감소가 관찰되었다. 무부하 4주 후, X-gal 표지 세포의 두드러진 두께 감소가 왼쪽 뒷다리에서 관찰되었으나 X-gal 표지 세포의 숫자는 양쪽 다리에서 유사하였다. RNA 시퀀싱 분석에서 총 315개의 유전자가 무부하 2주와 4주째 왼쪽 뒷다리에서 오른쪽 뒷다리에 비해 지속적인 발현의 감소를 보였다. 이 중 *Xirp2*, *AMPD1*, *Mettl11b*, *NEXN*, *CYP2E1*, *Bche*, *Ppp1r3c*, *Tceal7*, 그리고 *Gadl1* 유전자의 발현이 조골세포/골세포 분화 및 근육세포 분화 과정에서 증가됨을 실시간

PCR을 통해 확인하였다.

결론: 본 연구에서는 기계적 무부하가 쥐 생체 내 골손실의 이른 단계에서 성숙 조골세포가 골표면세포로 전환되는 과정을 가속화함을 확인하였다. 이러한 과정에서 유의미한 발현의 변화가 확인된 일부 유전자들은 향후 골다공증과 근감소증에 효과적인 약제의 표적으로서 규명될 잠재적 가능성이 있을 것으로 기대된다.

주요어: 기계적 무부하, 골표면세포, 유전자 발현 양상, 전사체

학 번: 2014-30933

이 논문의 일부 데이터는 Endocrinol Metab (Seoul) 2020;35:456-469에 게재되었습니다.